Water Resources Management (2023) 37:1481–1497
https://doi.org/10.1007/s11269-022-03419-3

NDVI Forecasting Model Based on the Combination of Time Series Decomposition and CNN – LSTM

Peiqiang Gao[1,2] · Wenfeng Du[1] · Qingwen Lei[3] · Juezhi Li[1,2] · Shuaiji Zhang[1,2] · Ning Li[1,2]

Received: 17 October 2022 / Accepted: 27 December 2022 / Published online: 15 February 2023

Abstract

Normalized difference vegetation index (NDVI) is the most widely used factor in the growth status of vegetation, and improving the prediction of NDVI is crucial to the advancement of regional ecology. In this study, a novel NDVI forecasting model was developed by combining time series decomposition (TSD), convolutional neural networks (CNN) and long short-term memory (LSTM). Two forecasting models of climatic factors and four NDVI forecasting models were developed to validate the performance of the TSD-CNN-LSTM model and investigate the NDVI's response to climatic factors. Results indicate that the TSD-CNN-LSTM model has the best prediction performance across all series, with the RMSE, NSE and MAE of NDVI prediction being 0.0573, 0.9617 and 0.0447, respectively. Furthermore, the TP-N (Temperature & Precipitation-NDVI) model has a greater effect than the T-N (Temperature-NDVI) and P-N (Precipitation-NDVI) models, according to the climatic factors-based NDVI forecasting model. Based on the results of the correlation analysis, it can be concluded that changes in NDVI are driven by a combination of temperature and precipitation, with temperature playing the most significant role. The preceding findings serve as a helpful reference and guide for studying vegetation growth in response to climate changes.

Keywords Normalized difference vegetation index · Climatic factors · Time series analysis · Prediction models · TSD-CNN-LSTM

✉ Wenfeng Du
duwf66@126.com

[1] State Key Laboratory of Coal Resources and Safe Mining, China University of Mining and Technology-Beijing, Beijing 100083, China

[2] College of Geoscience and Surveying Engineering, China University of Mining and Technology-Beijing, Beijing 100083, China

[3] School of Water Conservancy and Hydroelectric Power, Hebei University of Engineering, Handan, Hebei 056038, China

1 Introduction

Vegetation growth status as a critical indicator of regional ecosystem evaluation is affected by several factors, particularly in arid and semiarid regions (Jaber 2019; Herrmann et al. 2005; Liu et al. 2016). The response between vegetation and climatic factors is close, and climate change frequently causes differential changes in surface vegetation's temporal and spatial distribution (Jong et al. 2012; Pepin et al. 2015). According to previous research, temperature and precipitation are significant factors in arid and semi-arid areas (Na et al. 2021; Parizi et al. 2020; Cañón et al. 2011). Normalized difference vegetation index (NDVI), vegetation condition index (VCI), and vegetation health index (VHI) are currently the most widely used indices for vegetation drought studies (Alamdarloo et al. 2018). Where VCI and VHI are the new indices derived from NDVI that are used to study the effect of weather, moisture and temperature on vegetation (Kogan 1990; Pei et al. 2018; Tran et al. 2017). Meanwhile, NDVI is more commonly used as the preferred indicator of vegetation growth status in the study of vegetation growth in response climate changes (Bianchi et al. 2019; Wu et al. 2019).

In recent years, time series analysis has proliferated and plays a vital role in numerous application fields. Autoregressive Moving Average (ARMA) (Zarei and Mahmoudi 2020a), support vector regression (SVR) (Aghelpour et al. 2019), extreme learning machine (ELM) (Kuila et al. 2022), and artificial neural network (ANN) (Hu et al. 2021; Panwar et al. 2021) are popularly employed models. With the rapid advancement of artificial intelligence, convolutional neural network (CNN) and recurrent neural network (RNN) have become the most widely used deep neural networks, each with their advantages (Pérez-Alarcón et al. 2022). Due to its ability to efficiently extract input features, 1D CNN has become one of the most popular time series prediction techniques (Qiao et al. 2021; Qayyum et al. 2022). Long Short-Term Memory (LSTM) as a variant of RNN, is widely used in time series forecasting tasks due to its superior nonlinear fitting capability and low computational load (Tulensalo et al. 2020). However, there have been fewer studies on NDVI forecasting in the past two decades. Wang et al. (2015) simulated NDVI based on climatic factors using multiple linear regression. Huang et al. (2017) proposed an ANN and SVM-based combination forecasting model to improve the performance of NDVI prediction in the Yellow River Basin. Wu et al. (2019) utilized a time-delay neural network to predict NDVI in arid and semiarid grassland. Although the preceding model yielded superior results, these models are not suited for solving complex nonlinear problems and cannot mine internal time series features.

Detailed analysis of the internal characteristics of time series helps capture the precise variation trend, as seasonal and trend variables positively influence the model's prediction outcomes (Liu et al. 2020; Zarei and Mahmoudi 2020b; Zhang and Qi 2005). To extract seasonal and trend features from the original data, this paper introduces the X-12-Autoregressive integrated moving average (X-12-ARIMA) model (Hou 2021; Guo et al. 2018). Compared to other decomposition methods such as Seasonal-ARIMA (Parviz 2020), X-11-ARIMA (Pfeffermann and Sverchkov 2014), seasonal-trend decomposition procedures based on loess (STL) (Jiao et al. 2021), and empirical mode decomposition (EMD) (Malik et al. 2022), the X-12-ARIMA model improves the pre-processing based on the X-11-ARIMA model and is more extensively used in the seasonal adjustment analysis of time series (Su et al. 2021). Meanwhile, since deep learning relies primarily on historical data to recover the changing time series pattern to predict future variables, a reasonable selection of historical data can improve the model's prediction accuracy. Based on time series decomposition, R/S analysis was developed to determine the long-term correlation and the average cycle of trend components and to provide a rationale for selecting historical data (Zhang et al. 2018; Nikolopoulos et al. 2021).

For complex nonlinear processes caused by multiple elements, direct analysis of the original can't adequately reflect the patterns formed by the superposition of various features. On the other hand, time series decomposition of non-stationary NDVI series can effectively extract periodic and trend information caused by the deterministic factors and fluctuation information caused by random factors. CNN-LSTM eliminates the effects of random perturbations through filtering and feature extraction from TSD, allowing effective information to be transmitted downward and fitted. Based on TSD-CNN-LSTM, this study established two forecasting models of climatic factors (temperature and precipitation) and four forecasting models of NDVI. The primary goals of this paper are as follows: (1) validate the positive effect of internal feature analysis of time series on model's performance. (2) validate the universality of the TSD-CNN-LSTM algorithm for all series. (3) discuss the effect of temperature and precipitation on the NDVI.

2 Materials and Methods

2.1 Study Area

Ningtiaota coal mining region is located in the middle of Shenmu County, Shaanxi Province. The construction of the coal mine began in September 2005, the underground production equipment was put into operation in March 2009, and the first phase of mining in 2013. Most the region's landform units are wind-sand, loess hilly, and gully areas with a typical mid-temperate semiarid continental climate characterized by a cold winter, windy spring, hot summer, cool autumn, varying hot and cold seasons, a significant temperature difference between day and night, drought, little rainfall, and high evaporation. A thick layer of sand covers the area's surface, making it suitable for precipitation infiltration and conducive to groundwater recharge. Precipitation is most concentrated in July, August, and September, and precipitation is the primary source of recharge to the unconfined aquifer. The range of the study area is 110°10′30″E ~ 110°13′20″E, 38°57′20″N ~ 39°0′30″N, with a size of approximately 20 square kilometers (Fig. 1).

2.2 Data Processing

Landsat-5, landsat-7 and landsat-8 remote sensing data with a spatial resolution of 30 m × 30 m were downloaded from the United States Geological Survey (USGS) website. The National Earth System Science Data Center, National Science and Technology Infrastructure of China (http://www.geodata.cn). makes available climate data sets that include monthly temperature and cumulative precipitation with a global resolution of 2.5'. This study utilized monthly average temperature and precipitation data from 1961 to 2018 and monthly NDVI data from 2000 ~ 2018. NDVI values were calculated from GEE cloud platform, and finally get the long time series (Fig. 2 shows the variation curves from 2000 to 2018 of NDVI, temperature and precipitation series, which have high consistency). The calculation process is as follows:

$$NDVI_{vi} = \frac{NIR - Red}{NIR + Red} \tag{1}$$

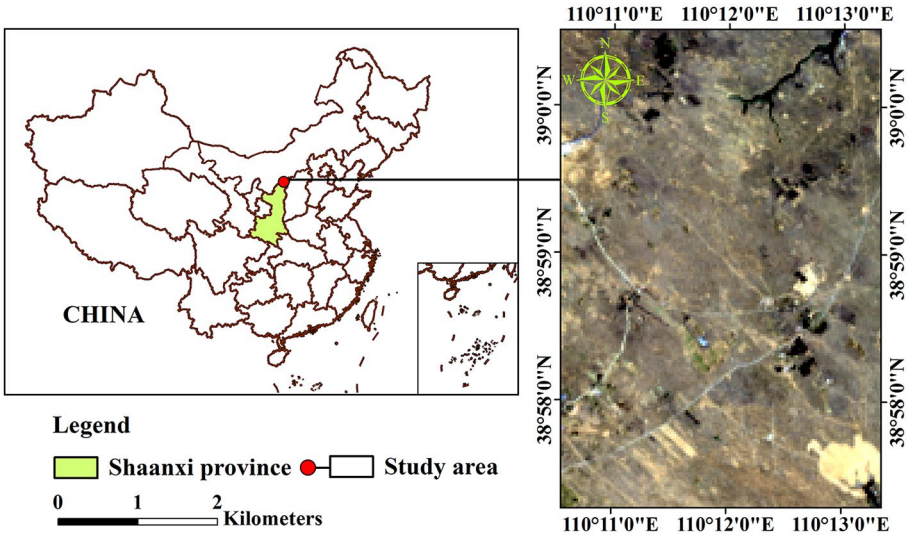

Fig. 1 Location of the study area

$$NDVI_{mean} = \frac{1}{n}\sum_{i=1}^{n} NDVI_{vi} \tag{2}$$

where *NIR* is the reflection value of the near-infrared channel, *Red* is the reflection value of the visible channel, n is the number of pixels of remote sensing image of the study area; vi represents the different pixels, $NDVI_{vi}$ represents the value of each pixel, and $NDVI_{mean}$ represents the mean value of all pixels.

2.3 X-12-ARIMA Algorithm

In 1998, Findley et al. added the pre-adjustment module to the X-11 method and introduced the X-12-ARIMA algorithm and accompanying procedures, which are widely used in the seasonal adjustment analysis of socioeconomic and other time series (Guo et al. 2018; Findley et al. 1998). In this study, the temperature, precipitation and NDVI series exhibit evident seasonal characteristics and an annual cycle, whereas the trend changes are not readily apparent. For time series decomposition, the additive model with three components was used (Su et al. 2021):

$$Y_t = T_t + S_t + R_t \tag{3}$$

where, Y_t represents the original series, T_t, S_t and R_t represent the trend components, seasonal components and residual components of time series at time t, respectively.

2.4 Rescaled Range Analysis

The time window τ of the input feature is a crucial parameter for network training because it reflects each subsequence feature's influence over the past τ months on the feature of the $\tau + 1$ month. If the time window is too large, it is possible to extract all pertinent

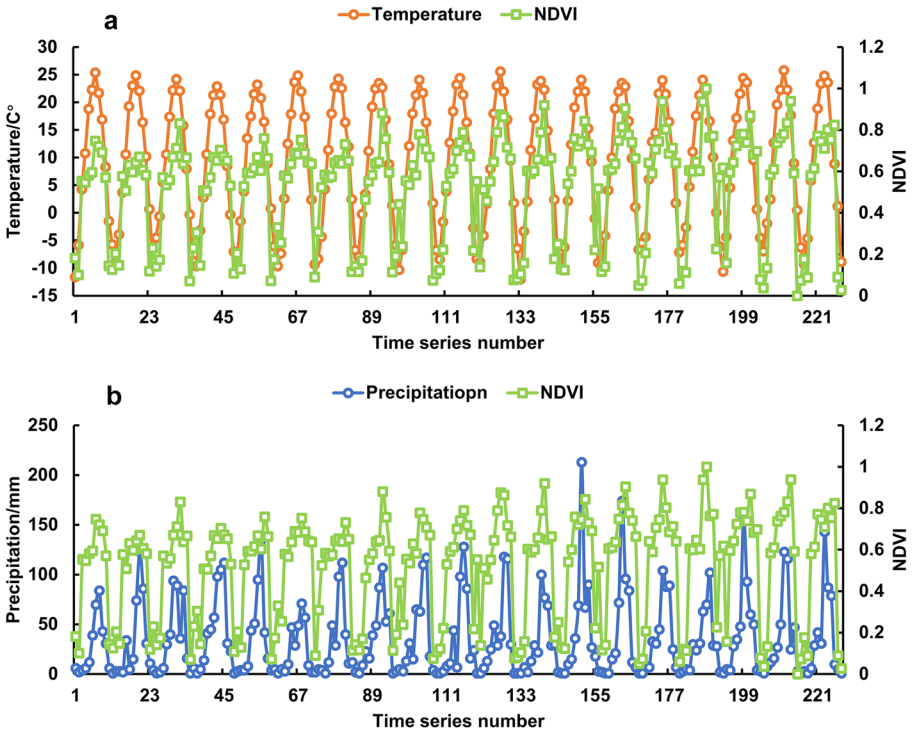

Fig. 2 Variation curves of monthly NDVI, temperature and precipitation in the Ningtiaota mining area from 2000 to 2018. **a** Variation curves of monthly NDVI and temperature. **b** Variation curves of monthly NDVI and precipitation

information from the time series, but it also introduces more random noise. On the other hand, if the time window is too small, the correlation between the response variables and the historical feature cannot be fully revealed. Therefore, R/S analysis is frequently used to describe the long-term correlation and average cycles of time series (Kalinin et al. 2018). In this study, R/S analysis is primarily used to determine the average cycles of the trend components and as a calculation basis for selecting time series feature windows (Zhang et al. 2018; He et al. 2015).

2.5 Proposed Model

2.5.1 CNN

Generally, 1D Convolutional Neural Networks (CNN) are employed for series processing (Barzegar et al. 2020). The typical structure of a CNN model primarily includes convolutional layer to extract the local data features; different convolution kernels are equivalent to different feature extractors. Batch Normalization makes the data pass down more effectively, while the pooling layer performs feature selection; the fully connected output layer is the final layer. Figure 3a illustrates the input time series of 1D CNN as an n*3 matrix; the red box represents the convolution size of a filter is 3*3, and

the 128 filters are convolved from top to bottom with a stride of 1. The extracted feature dimension after filter convolution is a (n-3 + 1)*3 matrix $C_1 \sim C_{n\text{-}2}$, eventually obtaining a 128*1 matrix after feature selection of the pooling process. The dimension of the feature is related to the input data dimension, the size of filter, and the convolution step.

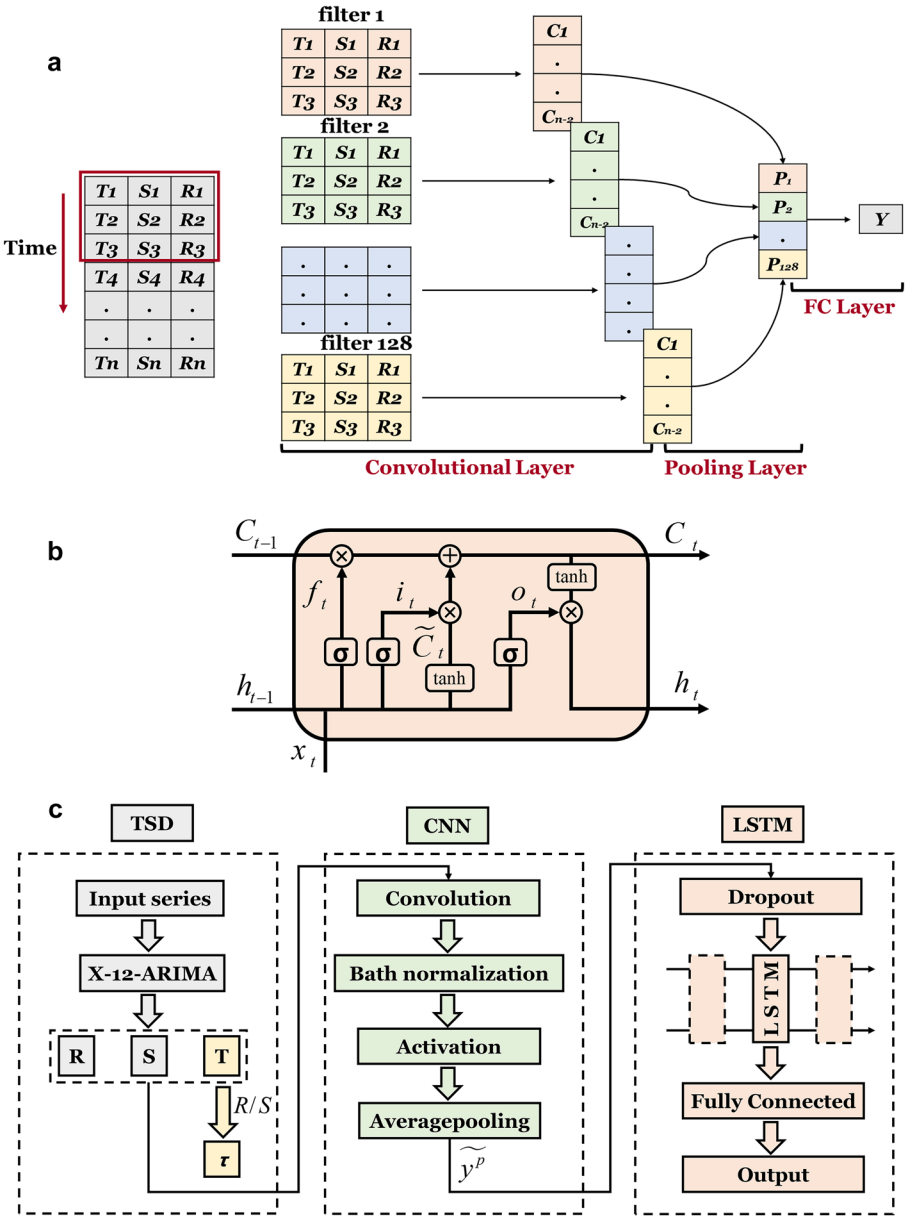

Fig. 3 **a** Convolution process of 1D CNN. **b** Structure of LSTM. **c** Structure of the TSD-CNN-LSTM

2.5.2 LSTM

Long Short-Term Memory (LSTM) neural network can effectively solve the gradient explosion and gradient disappearance issues that plague simple recurrent neural networks (Roy 2021; Rajesh et al. 2022). In Fig. 3b, c_t is the internal cell status introduced by the LSTM network for linear cyclic information transfer, which also outputs information nonlinearly to the external status h_t of the hidden layer. $\widetilde{c_t}$ is the candidate cell status obtained by the nonlinear function. The forget gate f_t controls how much information of internal cell status c_{t-1} must be forgotten at the previous moment: $f_t = \sigma(W_f x_t + U_f h_{t-1} + B_f)$. The input gate i_t controls how much information must be saved for the candidate cell status $\widetilde{c_t} = \tanh(W_c x_t + U_c h_{t-1} + b_c)$ at the current moment: $i_t = \sigma(W_i x_t + U_t h_{t-1} + b_i)$. The output gate o_t controls how much information of the internal cell status $c_t = f_t \odot c_{t-1} + i_t \odot \widetilde{c_t}$ at the current moment must be output to the external state $h_t = o_t \odot \tanh(c_t)$: $o_t = \sigma(W_o x_t + U_o h_{t-1} + b_o)$, where W and U represent the weight, b is the bias weight, and σ is the sigmoid function.

2.5.3 TSD-CNN-LSTM

CNN and LSTM models rely heavily on the historical information of the time window to restore the change rule of time series over time to predict the future response variables. TSD can extract the component features of the original time series using CNN to re-extract and filter the component features, which are then send to the LSTM network and output by the fully connected layer. Figure 3c depicts the structure and the calculation process of TSD-CNN-LSTM:

1. The original time series was decomposed into a group of feature vectors that included residual components, seasonal components, and trend components: $\{R_N, S_N, T_N\}$.
2. The mapping group of input feature of the convolution layer is a two-dimensional tensor $F \in \mathbb{R}^{\tau \times 3}$, where τ is the width of the mapping window of the input features of CNN. To calculate the feature map y_i^p of the output of the *ith* sample, the input feature maps F_i^1, F_i^2 and F_i^3 are convolutionally filtered with convolution kernels $W^{p,d}$.

$$F_i^T = \begin{bmatrix} F_i^1 \\ F_i^2 \\ F_i^3 \end{bmatrix} = \begin{bmatrix} T_{i-\tau}, T_{i-\tau+1}, \ldots, T_{i-1} \\ S_{i-\tau}, S_{i-\tau+1}, \ldots, S_{i-1} \\ R_{i-\tau}, R_{i-\tau+1}, \ldots, R_{i-1} \end{bmatrix} \tag{4}$$

$$\begin{gathered} Z_i^p = W^p \otimes F_i + b^p = \sum_{d=1}^{3} W^{p,d} \otimes F_i^d + b^p \quad \frac{-b \pm \sqrt{b^2 - 4ac}}{2a} \\ y_i^p = f(Z_i^p) \end{gathered} \tag{5}$$

where $T_{i-\tau}$, $S_{i-\tau}$ and $R_{i-\tau}$ represent the trend, seasonal and residual components of the past τ months at the time corresponding to the *ith* sample, respectively; $\otimes$ represents the cross-correlation operation (the convolution without flipping); $p = 1, \ldots, P$ represents the number of convolution kernels. b^p is the bias weight. $f(\cdot)$ is the Re*lu* function, which can solve the gradient disappearance problem and has a faster computational speed and convergence rate than tanh function and the sigmoid function, defined as Eq. (6):

$$Relu(x) = max(0, 1) \tag{6}$$

3. $\boldsymbol{y}_i^p$ is resampled by the pooling layer and output $\tilde{\boldsymbol{y}}^p$ after the convolution operation. This study utilizes average pooling for feature selection.
4. $\tilde{\boldsymbol{y}}^p$ enters the LSTM network to fit the time series relationship and outputs the predicted value from the fully connected layer. Dropout is an effective method to reduce model overfitting. During model training, neurons are removed from the neural network with a predetermined probability and reconnected when used. The mean square error is the loss function of parameter updating in a neural network.

$$MSE = \frac{1}{n}\sum_{i=1}^{m}(x_i - x_p)^2 \tag{7}$$

where x_i is the measured value corresponding to the *ith* training sample,x_p is the predicted value of the model, and n is the number of training samples.

2.6 Evaluation Indicators of Models

Root mean square error (*RMSE*), Nash–Sutcliffe efficiency coefficient (*NSE*), and Mean absolute error (*MAE*) evaluate the performance of the TSD-CNN-LSTM, TSD-CNN, TSD-LSTM and single LSTM models (Niazkar and Zakwan 2021; Zakwan 2019). *RMSE*, *NSE* and *MAE* are defined as:

$$RMSE = \sqrt{\frac{1}{n}\sum_{i=1}^{n}(x_i - x_{pi})^2} \tag{8}$$

$$NSE = 1 - \frac{\sum_{i=1}^{n}(x_i - x_{pi})^2}{\sum_{i=1}^{n}(x_i - \overline{x_i})^2} \tag{9}$$

$$MAE = \frac{1}{n}\sum_{i=1}^{n}\left|x_i - x_{pi}\right| \tag{10}$$

where n is the number of all test samples; x_i is the *ith* measured value; x_{pi} is the *ith* predicted value, and $\overline{x_i}$ is the mean of all test samples.

3 Results and Discussions

3.1 Time Series Decomposition

Temperature, precipitation, and NDVI series of the study area exhibit a clear annual cycle of seasonal characteristics. Figure 4 depicts the decomposition of temperature, precipitation and NDVI series into a seasonal component with an annual cycle, a trend component reflecting the change trend, and a residual component reflecting random fluctuations.

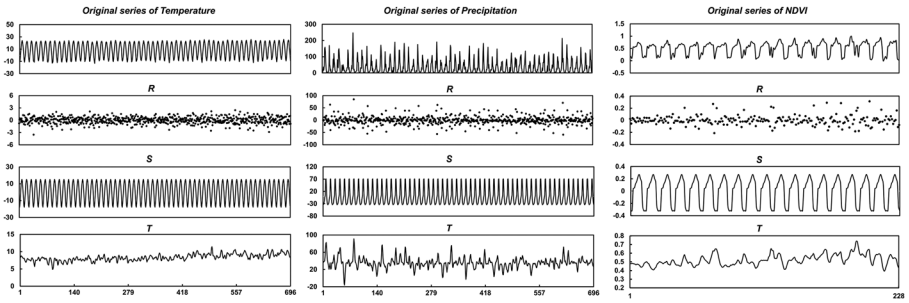

Fig. 4 Results of time series decomposition

According to the results of time series decomposition, the fluctuation ranges of residual component of the temperature series, precipitation series, and NDVI series are -3 ~ 3, -60 ~ 100 and -0.4 ~ 0.4, respectively, while the fluctuation ranges of the trend component are 5 ~ 10, -20 ~ 100 and 0.3 ~ 0.8, respectively. In summary, the trend component of temperature series exhibits more constant fluctuations than the precipitation and NDVI series.

3.2 Feature Window

Figure 5a–c show that the Hurst exponent of the trend components were $H_t = 0.95 > 0.5$, $H_p = 0.59 > 0.5$, and $H_{NDVI} = 0.84 > 0.5$, respectively. The results also indicate that all-time series have long-term correlations, which reflect exceptional memory in time series prediction. Figure 5d–f indicate that the average cycles of the trend components of temperature, precipitation and NDVI were obtained as $T_t = 33$, $T_p = 48$, and $T_{NDVI} = 16$, respectively. Since the seasonal cycles of temperature, precipitation and NDVI are all 12 months, which are entirely contained in the cycles of the trend components. Therefore, the feature windows of temperature, precipitation, and NDVI for network training are determined as $\tau_t = 33$, $\tau_p = 48$, $\tau_{NDVI} = 16$, respectively.

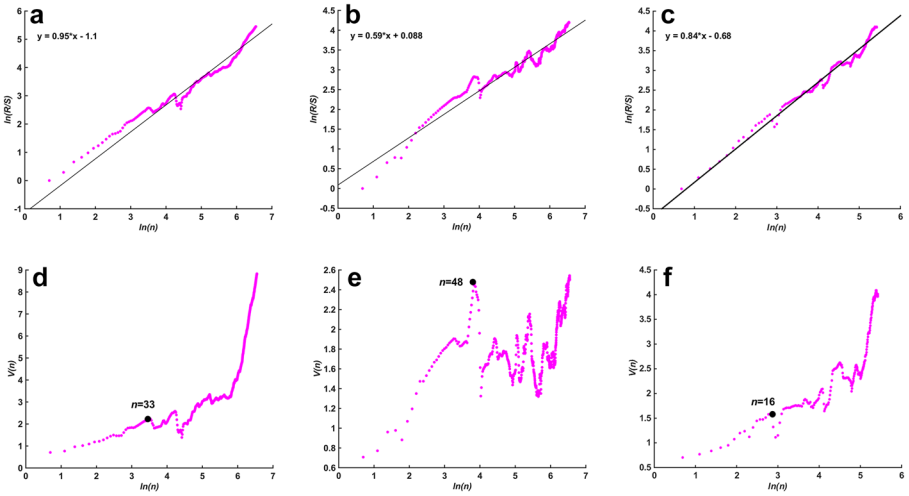

Fig. 5 Results of R/S analysis

3.3 Parameter Calibration

Depending on the size of the feature window, six models were established with an approximate 8:2 ratio of calibration sets to validation sets (Table 1 displays the internal network structure and parameters of TSD-CNN-LSTM models generated by the Anaconda platform.): (1) Temperature-Temperature (T-T) model; (2) Precipitation-Precipitation (P-P) model; (3) Temperature-NDVI (T-N) model; (4) Precipitation-NDVI (P-N) model; (5) Temperature & Precipitation-NDVI (TP-N) model; (6) NDVI-NDVI (N–N) model. Table 1 provides that the input size of T-T model is a 33*3 matrix, while that of the P-P model, the T-N model, the P-N model, the TP-N model and the N–N model is a 48*3 matrix, 33*3 matrix, 48*3 matrix, 48*6 matrix and 16*3 matrix, respectively.

3.4 Prediction Results

The effects of TSD-CNN-LSTM (TCL), TSD-CNN (TC), TSD-LSTM (TL), and single LSTM models on forecasting are depicted in Fig. 6. The T-T model has a marginally better fitting effect than the P-P and N–N models. In contrast, the N–N model fits significantly better than the T-N, P-N, and T&P-N models. Table 2 shows that the TSD-CNN-LSTM model of T-T and P-P models has the best forecasting performance with the smallest RMSE, MAE, and NSE, whereas the LSTM model has the worst forecasting performance. The T-N model's single LSTM model has the best prediction performance with the lowest RMSE and the highest NSE, while the P-N model's TSD-CNN-LSTM model has the best prediction performance with the lowest RMSE, MAE, and NSE. The TSD-CNN-LSTM model of T&P-N and N–N models has the best prediction performance with the smallest RMSE, MAE, and highest NSE, followed by the TSD-CNN and TSD-LSTM models, and the single LSTM model has the worst prediction performance.

3.5 Discussions

3.5.1 Validity of Data Pre-processing

In this paper, TSD-CNN-LSTM model demonstrated superior forecasting performance for all series compared to the TSD-CNN, TSD-LSTM and LSTM models. However, the single LSTM model had the worst performance among most models, possibly because a single RNN cannot effectively capture trend or seasonality in a time series (Bandara et al. 2020). The previous prediction has demonstrated that data pre-processing can improve the predictive accuracy of neural network models (Ni et al. 2020). Cui et al. (2020) have demonstrated that the prediction accuracy can be enhanced by detrending and de-seasonalizing the original time series. Zhang et al. (2022) established a CEEMDAN-LSTM model for water quality prediction based on the complete set of empirical mode decomposition (CEEMDAN) methods, which improved the precision of a single LSTM model. Wei and You (2022) improved the precipitation prediction accuracy of CNN and LSTM by capturing the time series details using the wavelet transform method. In light of the findings of this study, it is evident that data pre-processing is required prior to building a neural network model.

Table 1 Parameters of the established six models

Parameters	T-T		P-P		T-N		P-N		T&P-N		N–N	
Calibration set/year	1961–2008		1961–2018		2000–2017		2000–2017		2000–2017		2014–2017	
Validation set/year	2009–2018		2009–2018		2015–2018		2015–2018		2015–2018		2018	
Calibration length/month	543		528		180		180		180		164	
Validation length/month	120		120		48		48		48		48	
τ	33		48		33		48		48		16	
$\tau+1$	34		49		34		49		49		17	
Structure	Output shape	params	Output shape	params	Output shape	params	Output shape	params	Output shape	params	Output shape	params
Conv1D	(None,31,128)	1280	(None,46,128)	1280	(None,31,128)	1280	(None,46,128)	1280	(None,46,128)	2432	(None,14,128)	1280
Bath normalization	(None,31,128)	512	(None,46,128)	512	(None,31,128)	512	(None,46,128)	512	(None,46,128)	512	(None,14,128)	512
Activation	(None,31,128)	0	(None,46,128)	0	(None,31,128)	0	(None,46,128)	0	(None,46,128)	0	(None,14,128)	0
Pooling	(None,11,128)	0	(None,16,128)	0	(None,11,128)	0	(None,16,128)	0	(None,16,128)	0	(None,5,128)	0
Dropout	(None,11,128)	0	(None,16,128)	0	(None,11,128)	0	(None,16,128)	0	(None,16,128)	0	(None,5,128)	0
LSTM	(None, 128)	131584	(None, 128)	131584	(None, 128)	131584	(None, 128)	131584	(None, 128)	131584	(None, 128)	131584
Dropout1	(None, 128)	0	(None, 128)	0	(None, 128)	0	(None, 128)	0	(None, 128)	0	(None, 128)	0
Dense	(None,1)	129	(None,1)	129	(None,1)	129	(None,1)	129	(None,1)	129	(None,1)	129

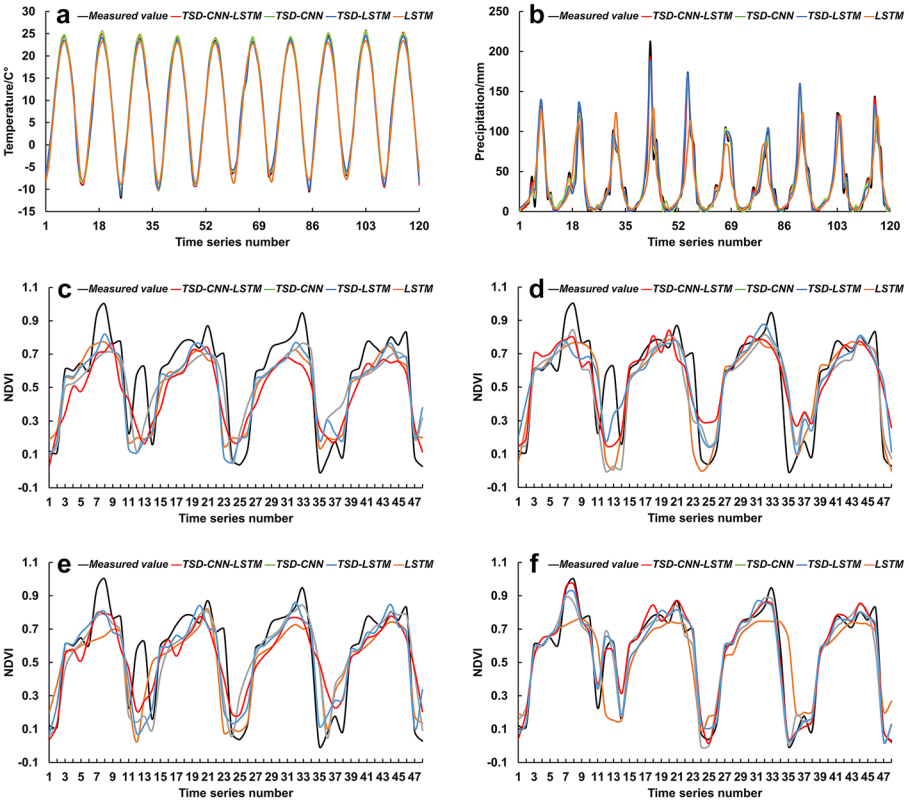

Fig. 6 Fitting curves of measured value and predicted value **a** T-T model. **b** P-P model. **c** T-N model. **d** P-N model. **e** TP-N model. **f** N–N model

3.5.2 Effect of Series Volatility on Prediction Results

According to the results of time series decomposition, the trend change of temperature, precipitation and NDVI series fluctuates with a small range of 5 ~ 10, significantly with a large range of -20 ~ 100, and irregularly with a small range of 0.3 ~ 0.8, respectively. Compared with the temperature series, the precipitation and NDVI series exhibit strong oscillations, and the characteristics of trend component are highly variable, which may explain why the prediction effects of the P-P and N–N models are marginally inferior to those of the T-T model (Yan 2012). The poor prediction performance of TSD-CNN-LSTM for the T-N model is likely attributable to the loss of information in the smoothly varying trend component, which the hybrid model may have caused. Additionally, the imbalance in training data significantly negatively impacts CNN's overall performance (Bandara et al. 2020; Hensman and Masko 2015).

3.5.3 Response of NDVI to Temperature and Precipitation

Correlation analysis of NDVI and climatic factors indicated that the multiple correlation coefficient between NDVI and temperature & precipitation is 0.833 ($P < 0.01$). The partial

Table 2 The RMSE, NSE and MAE of all models

Models		RMSE	NSE	MAE
T-T	TCL	0.4996	0.9981	0.4169
	TC	0.6513	0.9968	0.5255
	TL	0.623	0.9971	0.5115
	LSTM	1.4586	0.9839	1.1644
P-P	TCL	5.6941	0.9822	3.9855
	TC	8.5749	0.9596	6.347
	TL	7.7133	0.9673	5.532
	LSTM	24.6781	0.6654	14.4864
T-N	TCL	0.1719	0.6559	0.1219
	TC	0.1843	0.6043	0.1587
	TL	0.1726	0.6533	0.1421
	LSTM	0.1629	0.6909	0.1261
P-N	TCL	0.1688	0.6682	0.1191
	TC	0.1745	0.6454	0.1311
	TL	0.18	0.6229	0.1198
	LSTM	0.1863	0.5957	0.1152
TP-N	TCL	0.1607	0.6991	0.111
	TC	0.1726	0.6533	0.1346
	TL	0.1755	0.6411	0.1198
	LSTM	0.1974	0.5464	0.1389
N–N	TCL	0.0573	0.9617	0.0447
	TC	0.0619	0.9554	0.048
	TL	0.0815	0.9227	0.0629
	LSTM	0.1725	0.6535	0.1157

correlation coefficient between NDVI and temperature is 0.714 ($P<0.01$), while that between NDVI and precipitation is 0.01. The Pearson correlation between NDVI and temperature is 0.833 ($P<0.01$), while that between NDVI and precipitation is 0.611 ($P<0.01$). Previous research has demonstrated that vegetation growth in arid regions is more sensitive to climate change (Liu et al. 2016). Precipitation was primarily responsible for improving local vegetation in the arid Sahel region of Africa (Herrmann et al. 2005). While Lamchin et al. (2018) found that air temperature was the most influential factor in NDVI change in Asia from 1982 to 2014, Eamus et al. (2006) discovered that NDVI was negatively correlated with temperature and positively correlated with precipitation in Mongolia over the past three decades. Cui and Shi (2010) discovered that in eastern China, the response of vegetation to temperature change was more pronounced than its response to precipitation change. The factors that influence the NDVI in different regions vary. It is obvious that the driving factors of NDVI are different in different regions. Consequently, based on the results of the correlation analysis and prediction effects of NDVI models (N–N model > T&P-N model > T-N model > P-N model), it can be concluded that NDVI changes in the Ningtiaota coal mining area are most significantly driven by the combination of temperature and precipitation, with temperature playing the most critical role.

4 Conclusions

Changes in the NDVI are a complex nonlinear process caused by multiple factors. Direct analysis of the original series cannot fully reflect the patterns created by the superposition of multiple features. Decomposition of the non-stationary NDVI series can effectively extract the periodic and trend information from deterministic factors and the fluctuation information from stochastic factors. This paper proposes a new NDVI forecasting model based on TSD-CNN-LSTM that considers the nonlinear variation characteristic of the NDVI. In the meantime, two forecasting models of climatic factors and four forecasting models of NDVI were developed to test the model's generalizability and discuss the response of NDVI to climatic factors. Using RMSE, NSE and MAE to evaluate the performance of models, the results demonstrated that TSD could extract the residual, seasonal and trend change characteristics of the NDVI series, whereas R/S analysis can capture the trend characteristics based on TSD. The TSD-CNN-LSTM model can extract the most valuable historical information and perform optimal fitting with superior performance to the TSD-CNN, TSD-LSTM, and single LSTM models when combined with the CNN and LSTM models. The climatic factors-based NDVI forecasting models revealed that the T&P-N model had greater predictive ability than the T-N model, while the P-N model had the worst predictive ability. Using the results of the correlation analysis between NDVI and climatic factors, it is possible to conclude that the variation of NDVI was driven by both temperature and precipitation, with temperature playing a more significant role.

Nomenclature *NDVI*: Normalized difference vegetation index; *TSD*: Time series decomposition; *CNN*: Convolutional neural network; *LSTM*: Long short-term memory; *ARIMA*: Autoregressive integrated moving average; *R/S*: Rescaled range analysis; *TCL*: TSD-CNN-LSTM; *TC*: TSD-CNN; *TL*: TSD-LSTM; *T-T*: Temperature-Temperature; *T-N*: Temperature-NDVI; *P-N*: Precipitation-NDVI; *TP-N*: Temperature & Precipitation-NDVI.

Author Contribution Peiqiang Gao contributed to the research idea, methodology and model design as well as the writing of the paper. Wenfeng Du contributed to the research idea, methodology and paper review. Qingwen Lei contributed to the model design and methodology. Data collection and analysis were performed by Juezhi Li and Shuaiji Zhang. Ning Li contributed to research idea.

Funding This study was supported by the National Natural Science Foundation of Innovative Research Groups Project of Green, Intelligent and Safe Mining for Coal Resources (Grant Number: 52121003).

Availability of Data and Materials The data used to support the findings of this study are available from the corresponding author upon request.

Declarations

Competing Interests The authors declare no conflicts of interest.

References

Aghelpour P, Mohammadi B, Biazar SM (2019) Long-term monthly average temperature forecasting in some climate types of Iran, using the models SARIMA, SVR, and SVR-FA. Theor Appl Climatol 138(3–4):1471–1480. https://doi.org/10.1007/s00704-019-02905-w

Alamdarloo EH, Manesh MB, Khosravi H (2018) Probability assessment of vegetation vulnerability to drought based on remote sensing data. Environ Monit Assess 190:702. https://doi.org/10.1007/s10661-018-7089-1

Bandara K, Bergmeir C, Smyl S (2020) Forecasting across time series databases using recurrent neural networks on groups of similar series: A clustering approach. Expert Syst Appl 140. https://doi.org/10.1016/j.eswa.2019.112896

Barzegar R, Aalami MT, Adamowski J (2020) Short-term water quality variable prediction using a hybrid CNN–LSTM deep learning model. Stoch Env Res Risk A 34:415–433. https://doi.org/10.1007/s00477-020-01776-2

Bianchi E, Villalba R, Solarte A (2019) NDVI spatio-temporal patterns and climatic controls over northern Patagonia. Ecosystems 23(1):84–97. https://doi.org/10.1007/s10021-019-00389-3

Cañón J, Domínguez F, Valdes JB (2011) Vegetation responses to precipitation and temperature: a spatiotemporal analysis of ecoregions in the Colorado River Basin. Int J Remote Sens 32(20):5665–5687. https://doi.org/10.1080/01431161.2010.507259

Cui CL, Zhang W, Hong ZM, Meng LK (2020) Forecasting NDVI in multiple complex areas using neural network techniques combined feature engineering. Int J Digital Earth 13(12):1733–1749. https://doi.org/10.1080/17538947.2020.1808718

Cui L, Shi J (2010) Temporal and spatial response of vegetation NDVI to temperature and precipitation in eastern China. J Geogr Sci 20(2):163–176. https://doi.org/10.1007/s11442-010-0163-4

Eamus D, Fronend R, Loomes R, Hose G, Brad M (2006) A functional methodology for determining the groundwater regime needed to maintain the health of groundwater-dependent vegetation. Aust J Bot 54(2):97–114. https://doi.org/10.1071/BT05031

Findley DF, Monsell BC, Bell WR, Otto MC, Chen B-C (1998) New capabilities and methods of the X-12-ARIMA seasonal-adjustment program. J Bus Econ Stat 16(2):127–152

Guo HY, Chen QX, Xia Q, Kang CQ, Zhang X (2018) A monthly electricity consumption forecasting method based on vector error correction model and self-adaptive screening method. Int J Elec Power 95:427–439. https://doi.org/10.1016/j.ijepes.2017.09.011

He WP, Liu QQ, Jiang YD, Lu Y (2015) Comparison of performance between rescaled range analysis and rescaled variance analysis in detecting abrupt dynamic change. Chin Phys B 24(4):04920510. https://doi.org/10.1088/1674-1056/24/4/049205

Hensman P, Masko D (2015) The impact of imbalanced training data for convolutional neural networks. Degree Project in Computer Science, KTH Royal Institute of Technology, KTH Royal Institute of Technology

Herrmann SM, Anyamba A, Tucker CJ (2005) Recent trends in vegetation dynamics in the African Sahel and their relationship to climate. Glob Environ Change 15(4):394–404. https://doi.org/10.1016/j.gloenvcha.2005.08.004

Hou L (2021) Impact of COVID-19 on latent emissiveness of residents in China: Based on the X-12-ARIMA additive seasonal adjustment model. J Comput Methods Sci Eng 21:1591–1604. https://doi.org/10.3233/JCM-215473

Hu H, Zhang JF, Li T (2021) A novel hybrid decompose-ensemble strategy with a VMD-BPNN approach for daily streamflow estimating. Water Resour Manag 35:5119–5138. https://doi.org/10.1007/s11269-021-02990-5

Huang SZ, Ming B, Huang Q et al (2017) A case study on a combination NDVI forecasting model based on the entropy weight method. Water Resour Manag 31:3667–3681. https://doi.org/10.1007/s11269-017-1692-8

Jaber SM (2019) On the relationship between normalized difference vegetation index and land surface temperature: MODIS-based analysis in a semi-arid to arid environment. Geocarto Int 36(10):1117–1135. https://doi.org/10.1080/10106049.2019.1633421

Jiao F, Huang L, Song RJ, Huang HF (2021) An improved STL-LSTM model for daily bus passenger flow prediction during the COVID-19 pandemic. Sensors-Basel 21(17):5950. https://doi.org/10.3390/s21175950

Jong R, Verbesselt J, Schaepman ME, Bruin S (2012) Trend changes in global greening and browning: contribution of short-term trends to longer-term change. Glob Change Biol 18(2):642–655. https://doi.org/10.1111/j.1365-2486.2011.02578.x

Kalinin VV, Berg DB, Nazarova YY, Parusheva SS, Dolganov AN (2018) R/S-analysis of cash-flow: Cases of business eco community and separate enterprise. Aip Conf Proc 2040:050015. https://doi.org/10.1063/1.5079113

Kogan FN (1990) Remote sensing of weather impacts on vegetation in non-homogeneous areas. Int J Remote Sens 11(8):1404–1419. https://doi.org/10.1080/01431169008955102

Kuila S, Dhanda N, Joardar S (2022) ECG signal classification and arrhythmia detection using ELM-RNN. Multimed Tools Appl. https://doi.org/10.1007/s11042-022-11957-6

Lamchin M, Lee W-K, Jeon SW, WangSW LCH, Song C, Sung MJ (2018) Long-term trend and correlation between vegetation greenness and climate variables in Asia based on satellite data. Sci Total Environ 618:1089–1095. https://doi.org/10.1016/j.scitotenv.2017.09.145

Liu S, Ji H, Wang MC (2020) Nonpooling convolutional neural network forecasting for seasonal time series with trends. Ieee T Neur Net Lear 31(8):2879–2888. https://doi.org/10.1109/Tnnls.2019.2934110

Liu YX, Wang YL, Du YY, Zhao MY, Peng J (2016) The application of polynomial analyses to detect global vegetation dynamics during 1982–2012. Int J Remote Sens 37(7):1568–1584. https://doi.org/10.1080/01431161.2016.1142688

Malik SA, Parah SA, Malik BA (2022) Power line noise and baseline wander removal from ECG signals using empirical mode decomposition and lifting wavelet transform technique. Health Technol-Ger. https://doi.org/10.1007/s12553-022-00662-x

Na R, Na L, Du H, He HS, Shan Y, Zong S, Huang L, Yang Y, Wu Z (2021) Vegetation greenness variations and response to climate change in the arid and semi-arid transition zone of the mongo-lian plateau during 1982–2015. Remote Sens 13(20). https://doi.org/10.3390/rs13204066

Ni LL, Wang D, Singh VP, Wu JF, Wang YK, Tao YW (2020) Streamflow and rainfall forecasting by two long short-term memory-based models. J Hydrol 583:124296. https://doi.org/10.1016/j.jhydrol.2019.124296

Niazkar M, Zakwan M (2021) Application of MGGP, ANN, MHBMO, GRG, and linear regression for developing daily sediment rating curves. Math Probl Eng. https://doi.org/10.1155/2021/8574063

Nikolopoulos D, Moustris K, Petraki E, Cantzos D (2021) Long-memory traces in PM10 time series in Athens, Greece: investigation through DFA and R/S analysis. Meteorol Atmos Phys 133(2):261–279. https://doi.org/10.1007/s00703-020-00744-3

Panwar VS, Pandey A, Hasan ME (2021) Generalised regression neural network (Grnn) architecture-based motion planning and control of an e-puck robot in V-Rep software platform. Acta Mech Autom 15(4):209–214. https://doi.org/10.2478/ama-2021-0027

Parizi E, Hosseini SM, Ataie-Ashtiani B, Simmons CT (2020) Normalized difference vegetation index as the dominant predicting factor of groundwater recharge in phreatic aquifers: case studies across Iran. Sci Rep 10(1):17473. https://doi.org/10.1038/s41598-020-74561-4

Parviz L (2020) Comparative evaluation of hybrid SARIMA and machine learning techniques based on time varying and decomposition of precipitation time series. J Agr Sci Tech-Iran 22(2):563–578

Pei FS, Wu CJ, Liu XP, Li X, Yang KQ, Zhou Y, Wang K, Xu L, Xia GR (2018) Monitoring the vegetation activity in China using vegetation health indices. Agr Forest Meteorol 248:215–227. https://doi.org/10.1016/j.agrformet.2017.10.001

Pepin N, Bradley RS, Diaz HF et al (2015) Elevation-dependent warming in mountainregions of the world. Nat Clim Change 5(5):424–430. https://doi.org/10.1038/NCLIMATE2563

Pérez-Alarcón A, Garcia-Cortes D, Fernández-Alvarez JC, Martínez-González Y (2022) Improving monthly rainfall forecast in a watershed by combining neural networks and autoregressive models. Environ Process 9:53. https://doi.org/10.1007/s40710-022-00602-x

Pfeffermann D, Sverchkov M (2014) Estimation of mean squared error of X-11-ARIMA and other estimators of time series components. J Off Stat 30(4):811–838. https://doi.org/10.2478/Jos-2014-0049

Qayyum A, Khan MKAA, Benzinou A, Mazher M, Ramasamy M, Aramugam K, Deisy C, Sridevi S, Suresh M (2022) An efficient 1DCNN-LSTM deep learning model for assessment and classification of fMRI-based autism spectrum disorder. Lect Note Data Eng 96:1039–1048. https://doi.org/10.1007/978-981-16-7167-8_77

Qiao YH, Wang Y, Ma CX, Yang J (2021) Short-term traffic flow prediction based on 1DCNN-LSTM neural network structure. Mod Phys Lett B 35(2):2150042. https://doi.org/10.1142/S0217984921500421

Rajesh M, Anishka S, Viksit PS, Arohi S, Rehana S (2022) Improving short-range reservoir inflow forecasts with machine learning model combination. Waetr Resour Manag. https://doi.org/10.1007/s11269-022-03356-1

Roy DK (2021) Long short-term memory networks to predict one-step ahead reference evapotranspiration in a subtropical climatic zone. Environ Process 8:911–941. https://doi.org/10.1007/s40710-021-00512-4

Su T, Feng TC, Huang BH, Han ZX, Qian ZH, Feng GL, Hou W (2021) Trend, seasonal, and irregular variations in regional actual evapotranspiration over china: A multi-dataset analysis. Front Phys 9(718771). https://doi.org/10.3389/fphy.2021.718771

Tran HT, Campbell JB, Tran TD, Tran HT (2017) Monitoring drought vulnerability using multispectral indices observed from sequential remote sensing (case study: Tuy Phong, Binh Thuan, Vietnam). Gisci Remote Sens 54(1):167–184. https://doi.org/10.1080/15481603.2017.1287838

Tulensalo J, Seppanen J, Ilin A (2020) An LSTM model for power grid loss prediction. Electr Pow Syst Res 189:106823. https://doi.org/10.1016/j.epsr.2020.106823

Wang S, Huang GH, Huang W et al (2015) A polynomial chaos ensemble hydrologic prediction system for efficient parameter inference and robust uncertainty assessment. J Hydrol 529:1129–1146. https://doi.org/10.1016/j.jhydrol.2015.10.021

Wei M, You XY (2022) Monthly rainfall forecasting by a hybrid neural network of discrete wavelet transformation and deep learning. Water Resour Manag 36:4003–4018. https://doi.org/10.1007/s11269-022-03218-w

Wu TS, Fu HP, Feng F, Bai HM (2019) A new approach to predict normalized difference vegetation index using time-delay neural network in the arid and semi-arid grassland. Int J Remote Sens 1–14. https://doi.org/10.1080/01431161.2019.1624870

Yan W (2012) Toward automatic time-series forecasting using neural networks. IEEE Trans Neural Netw Learn Syst 23(7):1028–1039. https://doi.org/10.1109/TNNLS.2012.2198074

Zakwan M (2019) Comparative analysis of the novel infiltration model with other infiltration models. Water Environ J 33(4):620–632. https://doi.org/10.1111/wej.12435

Zarei AR, Mahmoudi MR (2020a) Ability assessment of the stationary and cyclostationary time series models to predict drought indices. Water Resour Manag 34(15):5009–5029. https://doi.org/10.1007/s11269-020-02710-5

Zarei AR, Mahmoudi MR (2020b) Investigating the ability of periodically correlated (PC) time series models to forecast the climate index. Stoch Env Res A 34(1):121–137. https://doi.org/10.1007/s00477-019-01751-6

Zhang GP, Qi M (2005) Neural network forecasting for seasonal and trend time series. Eur J Oper Res 160(2):501–514. https://doi.org/10.1016/j.ejor.2003.08.037

Zhang J, Hu QW, Wang SH, Ai MY (2018) Variation trend analysis of runoff and sediment time series based on the R/S Analysis of simulated loess tilled slopes in the Loess Plateau, China. Sustainability-Basel 10(1):32. https://doi.org/10.3390/su10010032

Zhang L, Jiang ZQ, He SS, Duan JF, Wang PF, Zhou T (2022) Study on water quality prediction of urban reservoir by coupled CEEMDAN decomposition and LSTM neural network mode. Water Resour Manag 36:3715–3735. https://doi.org/10.1007/s11269-022-03224-y